JGR Oceans

RESEARCH ARTICLE
10.1029/2019JC015022

Special Section:
Forum for Arctic Modeling and Observational Synthesis (FAMOS) 2: Beaufort Gyre phenomenon

On the Origin of Water Masses in the Beaufort Gyre

S. J. Kelly[1,2], A. Proshutinsky[3], E. K. Popova[1], Y. K. Aksenov[1], and A. Yool[1]

[1]National Oceanography Centre, Southampton, UK, [2]University of Southampton, Southampton, UK, [3]Woods Hole Oceanographic Institution, Falmouth, MA, USA

Abstract The Beaufort Gyre is a key feature of the Arctic Ocean, acting as a reservoir for freshwater in the region. Depending on whether the prevailing atmospheric circulation in the Arctic is anticyclonic or cyclonic, either a net accumulation or release of freshwater occurs. The sources of freshwater to the Arctic Ocean are well established and include contributions from the North American and Eurasian Rivers, the Bering Strait Pacific water inflow, sea ice meltwater, and precipitation, but their contribution to the Beaufort Gyre freshwater accumulation varies with changes in the atmospheric circulation. Here we use a Lagrangian backward tracking technique in conjunction with the 1/12-degree resolution Nucleus for European Modelling of the Ocean model to investigate how sources of freshwater to the Beaufort Gyre have changed in recent decades, focusing on increase in the Pacific water content in the gyre between the late 1980s and early 2000s. Using empirical orthogonal functions we analyze the change in the Arctic oceanic circulation that occurred between the 1980s and 2000s. We highlight a "waiting room" advective pathway that was present in the 1980s and provide evidence that this pathway was caused by a shift in the center of Ekman transport convergence in the Arctic. We discuss the role of these changes as a contributing factor to changes in the stratification, and hence potentially the biology, of the Beaufort Gyre region.

Plain Language Summary The Beaufort Gyre, a clockwise ice and water circulation in the Arctic Ocean, is an important feature of the Arctic because it stores a large volume of fresh—relative to the rest of the ocean—water. Depending on the atmospheric circulation driving it, the Beaufort Gyre can either accumulate or release this freshwater. The sources of relatively freshwater to the Beaufort Gyre are Arctic rivers, the Bering Strait, and melting sea ice. By tracking virtual particles in a high-resolution ocean model, we investigate how these sources have changed in recent decades, and identify a change in the pathways bringing them to the Beaufort Gyre. This change in ocean circulation was found to correlate with a change in the mixed layer depth in the model.

Key Points:
- Lagrangian particle tracking technique used to investigate advective pathways associated with different sources of Beaufort Gyre water
- Change in advective pathways associated with Pacific inflow to the gyre occurred between 1980s and 2000s
- This change in pathways correlates with a shoaling of the modeled mixed layer depth in the Beaufort Gyre region

Supporting Information:
- Supporting Information S1

Correspondence to:
S. J. Kelly,
s.kelly@soton.ac.uk

Citation:
Kelly, S. J., Proshutinsky, A., Popova, E. K., Aksenov, Y. K., & Yool, A. (2019). On the origin of water masses in the Beaufort Gyre. *Journal of Geophysical Research: Oceans*, *124*, 4696–4709. https://doi.org/10.1029/2019JC015022

Received 31 JAN 2019
Accepted 18 JUN 2019
Accepted article online 26 JUN 2019
Published online 9 JUL 2019

1. Introduction

The Beaufort Gyre is an anticyclonic oceanic gyre in the Canada Basin that stores a large volume of freshwater in the Arctic Ocean, and as such has a significant role in freshwater accumulation in the Arctic, changing upper ocean stratification and, potentially, affecting sea ice retreat and the dynamics of the Arctic Ocean as a whole (Aksenov et al., 2016; Mcphee et al., 2009). In order to understand how the Arctic Ocean has changed in recent decades, as well as how it may change in the future, it is vital to understand the mechanisms of the freshwater accumulation, specifically advective pathways of the freshwater in the Beaufort Gyre. Changes in circulation pathways are important for bringing different, potentially warmer, and less dense water masses to the Beaufort Gyre (Aksenov et al., 2017; Karcher et al., 2012), which in turn can change stratification and mixed layer depth, modifying the nutrient content of the region (Popova et al., 2013). Stronger stratification inhibits mixing (Rippeth et al., 2015) and reduces the amount of nutrients that can be brought to the upper ocean where there is sufficient light penetration in summer and phytoplankton can grow. Weakening of the stratification, on the other hand, promotes mixing and hence increased biogeochemical activity (Carmack et al., 2016). Changes in stratification and mixing affect heat transfer from the intermediate depth Atlantic Water (AW) to the surface (Polyakov et al., 2010; Polyakov et al., 2017): a more strongly stratified ocean allows less heat to be brought to the surface (and vice versa), thus may play an important role in sea ice retreat in all seasons in the next few decades (Aksenov et al., 2017; Polyakov et al., 2010; Stroeve et al., 2018). For these reasons, studying the changes in advective pathways of water masses can provide valuable insight into understanding a contributing factor to changes in the dynamics and biogeochemistry of the Beaufort Gyre and the Arctic Ocean as a whole.

Previous work (Giles et al., 2012; Polyakov et al., 1999; Proshutinsky et al., 1999) has established that the net accumulation or release of freshwater in the Beaufort Gyre is largely driven by quasi-decadal oscillating patterns in the wind forcing. The ocean's response to these variations is a pronounced bimodal state of the Arctic Ocean with stronger or weaker Beaufort Gyre, that is, the Arctic Ocean Oscillation (AOO) index (hereafter AOO). Proshutinsky and Johnson (1997) define the AOO from changes in sea surface heights using a coupled ice-ocean shallow-water barotropic model. The AOO describes whether the barotropic component of the circulation is dominated by cyclonic or anticyclonic motion, with the former shown (Proshutinsky et al., 2002; Proshutinsky et al., 2009) to correlate with release of freshwater from the Beaufort Gyre and the latter associated with freshwater accumulation.

A net increase in Beaufort Gyre freshwater content has been observed over the two decades between 1992 and 2012, with increased precipitation and melting of sea ice contributing factors to this (Krishfield et al., 2014; Proshutinsky et al., 2009; Rabe et al., 2014). Meteoric water (riverine input, glacial melt, and precipitation minus evaporation) also contributes to the freshwater budget of the Arctic Ocean. The meteoric water imports/exports to the Arctic Ocean are approximately balanced (Alkire et al., 2017), suggesting that the observed freshwater increase in the Canada Basin is due to a spatial redistribution of freshwater across the Arctic (Alkire et al., 2017; Wang et al., 2019). The mechanism driving the accumulation of freshwater during anticyclonic atmospheric forcing is Ekman pumping (Aksenov et al., 2016; Proshutinsky et al., 2002; Proshutinsky et al., 2009). Anticyclonic wind drives an Ekman transport to convergence which results in the observations of increasingly domed sea surface heights in the Beaufort Gyre (Armitage et al., 2016; Giles et al., 2012).

Since 1948, the AOO has typically varied with a period of approximately 10–15 years up until 1996. However, this relationship has broken down in recent years, with the AOO being in the anticyclonic circulation regime since 1997 until 2015 and beyond (Proshutinsky et al., 2015). In addition to quasi-oscillatory variability in the Arctic, anthropogenic climate change is having secular effect on the region: "Arctic amplification" of global warming is seeing temperatures in the polar region increase twice as rapidly as the rest of the world ocean (Cao et al., 2017; Cohen et al., 2014; Graversen et al., 2008). Historically, the Beaufort Gyre has played a "flywheel" role in influencing the dynamics of the Arctic Ocean as a whole (Proshutinsky et al., 2002), maintaining the negative salinity anomaly in the region and facilitating the dominant anticyclonic geostrophic circulation in the Canada Basin throughout the year, even when the wind forcing becomes cyclonic.

While accumulation of freshwater, and in particular a freshening of the upper mixed layer in the Beaufort Gyre region can act to make the ocean more strongly stratified, there is a competing influence in the form of sea ice cover. Sea ice mediates the reaction between the atmosphere and ocean which limits how much wind-driven mixing is possible in the Arctic. With Arctic sea ice rapidly declining, and ice-free summers predicted by midcentury (Boe et al., 2009; Overland & Wang, 2013; Wang & Overland, 2012), more open water allows for increased wind driven mixing and hence would counter the effect of freshwater accumulation and decrease the stratification in the Beaufort Gyre region. These dynamical processes compete with thermodynamic mechanisms which increase the thickness of the mixed layer in winter (during intense new ice formation in the regions free of ice during summer) and increase water stratification in summer due to ice melt and direct heating of the upper ocean layers by solar radiation.

Here we aim to investigate how the advective pathways bringing freshwater to the Beaufort Gyre region have altered during this period of rapid change for the Arctic Ocean. We then discuss the role of these dynamic changes in potentially contributing (alongside other, thermodynamic processes) to changes in stratification and mixing in the Beaufort Gyre region, and the potential impact for the biology of the region.

We aim to address three main questions. First, how have the sources of water to the Beaufort Gyre changed since 1980? Second, how have the advective pathways bringing Pacific water to the gyre changed? And third, what is causing this change? Additionally, we investigate variability in the modeled mixed layer depth across the Arctic over the same period. We discuss the link between this and the change in circulation pathways as a potential contributing factor to variations in the mixed layer depth.

2. Methodology

2.1. Nucleus for European Modelling of the Ocean Model and ARIANE Particle Tracking

The model used in experiments here is the Nucleus for European Modelling of the Ocean (NEMO), coupled to the Louvain-la-Neuve Ice Model (LIM2) sea ice model (Fichefet & Maqueda, 1997; Goosse & Fichefet, 1999; Madec, 2014). This version of NEMO has 75 depth levels (31 of which are in the top 200 m, with resolution as fine as 1 m in the uppermost layer), and has a horizontal resolution of approximately 1/12°, giving it a grid length-scale of 3–5 km in the Arctic, making it eddy permitting throughout the Arctic, though not fully eddy resolving on the shelves (Nurser & Bacon, 2014). NEMO is forced at the air-sea interface using the version 5.2 DRAKKAR forcing set (Brodeau et al., 2010). This includes 6-hourly winds, temperature and humidity from ERA40 reanalysis, daily longwave and shortwave radiative fluxes, and monthly means for precipitation and river runoff from CORE2 reanalysis. The DRAKKAR forcing set utilizes a monthly climatology for riverine input (Brodeau et al., 2010; Timmermann et al., 2005), with freshwater added at the surface level in this configuration of NEMO. The model was run with this DRAKKAR forcing set forcing between 1958 and 2015.

For our experiments, we use the ARIANE software (Blanke & Raynaud, 1997) using model output from NEMO. ARIANE works off-line, reading in the 3-D velocity fields saved in the NEMO output, interpolating to solve for particle translation through model grid cells, and saving particle positions daily. The output from the global NEMO model used here (run ORCA0083-N006) is saved as five-day means. ARIANE can be run both forward and backward in time, and it is the backward tracking that we employ here.

ARIANE, or other Lagrangian packages, are an especially useful tool for investigating the results of high-resolution ocean models where running the full model with online tracers would be prohibitively computationally expensive. However, this approach does have limitations. Small-scale processes such as diffusion and mixing, which are parameterized in the model, cannot straightforwardly be factored into Lagrangian analysis when investigating advective pathways (Wagner et al., 2019).

The NEMO-LIM2 model and ARIANE software are more completely described in Kelly et al. (2018), where validation of the surface circulation in this model configuration was performed. Comparing modeled sea surface heights (SSH), observed SSH (Armitage et al., 2016), and the barotropic streamfunction of modeled circulation showed good agreement between the data sets. Additionally, empirical orthogonal function (EOF; see section 2.3) analysis of modeled and observed SSH over the period 2003–2012 shows the same dominant nonseasonal mode of variability in the region observed by satellite (see supporting information; Armitage et al., 2016).

NEMO has previously been validated extensively in the Arctic Ocean. For instance, modeled stratification and water mass types show good agreement with observed Arctic stratification for other NEMO configurations (Aksenov et al., 2016; Janout et al., 2015; Luneva et al., 2015). Additional validation of the modeled mixed layer in the 1/12-degreeconfiguration of NEMO used here is provided in the supporting information to this paper. There we compare the modeled mixed layer depth to that found in observations (Peralta-Ferriz & Woodgate, 2015), and find good model skill. The largest discrepancy was found to be an overestimate of the summer mixed layer depth in the Barents Sea, away from the focus of this research.

Previous work has used ARIANE in conjunction with various different configurations of the NEMO model in the Arctic Ocean. Lique et al. (2010) used a global ¼-degree ORCA025 configuration together with a backtracking approach to assess the sources of water exiting the Arctic Ocean via the Fram and Davis Straits. Hu and Myers (2013) used a regional Arctic configuration of NEMO alongside ARIANE to investigate Pacific water inflow pathways during a model spin-up, producing inflow pathways consistent with more recent online passive tracer experiments (Aksenov et al., 2016). Finally, Kelly et al. (2018) investigated advective pathways in the context of pollutant spills from the Northern Sea route using ARIANE in conjunction with the same 1/12 global NEMO model used here.

2.2. Lagrangian Experiment Design Modal Experiments

The sources of freshwater for the Arctic Ocean are well established: Siberian and Alaskan Rivers, Pacific Ocean inflow, sea ice meltwater, and precipitation (e.g., (Aagaard & Carmack, 1989). Less is known about the advective pathways associated with these sources and, in particular, the freshwater components by

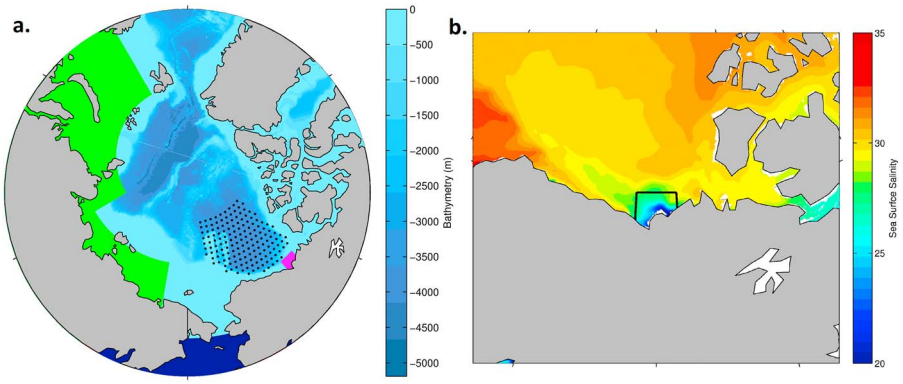

Figure 1. (*a*) Experiment design. Black dots show the Beaufort Gyre (BG) region where particles were initialized at five different depth levels. The colored regions represent the traps used to define sources of BG water, as used for classifying Lagrangian trajectories: Pacific (dark blue), Eurasia (green), and Mackenzie River (magenta). Background color scale shows bathymetry. *(b)* Modeled sea surface salinity (1997 annual mean—illustrative choice of a year with approximately neutral AOO conditions) in the Mackenzie River region, used to define the Mackenzie River "trap." The black box in Figure 1b is the same as the magenta box from Figure 1a.

sources in the Beaufort Gyre region. Thus, the goal of this work is to use a Lagrangian particle tracking technique, in conjunction with a high-resolution ocean model, to investigate water mass (particles representing them) pathways and their temporal variability.

We conducted a set of numerical experiments focusing on the origin of the water in the Beaufort Gyre. To investigate this, we release "particles" throughout the Beaufort Gyre region, and, using the ARIANE software, track them backward for 10 years to their sources. Ten years was chosen to ensure that the majority of particles would have left the gyre within the experiment—this, rather than the time scaleto reach each source—is the limiting factor in the experiment. This approach allows us to attribute fractions of the freshwater to the Mackenzie River, Pacific Ocean, and Eurasian shelf, but it does not permit investigation of pathways associated with meltwater or precipitation.

Our Lagrangian particles were initially uniformly distributed over a region bounded by 169°W, 129°W, 81°N, and a southern boundary taken to be the 300-m depth contour (see Figure 1a for each horizontal release location). We define this to be our "Beaufort Gyre region." Particles were released at five depth levels: 1, 21, 44, 82, and 140 m (chosen to correspond to integer depth levels in NEMO that sample different layers of the Beaufort Gyre). One particle was released at each horizontal location (total of 156 per depth level) and each depth to give a total of 780 particles per release. Releases were performed monthly between 1980 and 2013 (giving a grand total of 9,360 particles per year), and each particle's location was recorded daily for 10 years. Since particle trajectories were followed backward in time, NEMO output was required for the period 1970 to 2013.

Because of the large number of trajectories in our experimental design, we employ "traps" in our analysis to establish specific pathways taken by trajectories. This enables us to log their timing and quantity through particular regions. Essentially, for each simulated time point, we automatically determine whether trajectories are located within a series of small domains: the traps. We have positioned these in the locations of known circulation pathways, and where they permit clearly distinct routes to be distinguished. Three traps were used in this experiment, to identify particles which were tracked back to three different sources: Pacific, Eurasia, and the Mackenzie River. See Figure 1 for a visual representation of these traps.

Particles of Pacific origin are straightforward to define—any particle with a recorded position south of 65°N and with longitude between 150°E and 150°W was classified as Pacific. Second, any particles which were tracked back to a trap south of 75°N and between 120°E and 170°E or south of 80°N and between 30°E and 120°E were marked as originating from the Eurasian shelf. Third, a trap based on the plume of the Mackenzie River was defined—particles (which had not already been attributed to either the Pacific or Eurasia) were considered of Mackenzie origin if they spent at least one time step between 68°N and 70.5°N and between 132°W and 138°W (see Figure 1b).

In addition to our three traps, we counted the number of particles which still remain in our Beaufort Gyre region (as defined previously) after 10 years of backtracking, as well as the number of particles which did leave the gyre but were not attributed to any of the three sources using the methodology described above. These are assumed to either have not left the gyre (due to our rather strict definition of the Beaufort Gyre region) or to be en route to one of the other traps at the time the experiment ended.

2.3. Analysis Techniques

First, we compare the number of particles tracked back to each source for each year of particle releases. Second, we investigate the subset of particles which originate from the Pacific Ocean separately to highlight a change in advective pathways. For the Pacific, we calculate the year in which particles cross the Bering Strait (regardless of when they were initially seeded in the Beaufort Gyre.) Then, looking at each of the five release depths individually, we calculate the concentration of particles throughout the Arctic for particles that cross the Bering Strait in each year. EOF analysis is then performed to compare how these concentrations vary between years.

EOF analysis is a widely employed technique that can be used with spatial and temporal data to highlight different modes of variability which are independent (orthogonal) of each other. It has been used in various Arctic studies, for example, in the context of observed SSH patterns across the Arctic (Armitage et al., 2016), and we use the EOF technique to investigate modeled changes in SSH here. This method is particularly useful for identifying temporal trends and determining whether spatial areas vary in or out of phase with one another.

This is achieved by taking a three-dimensional variable (latitude, longitude, and time), and, by an orthogonal transformation, converting it into eigenvalues and eigenvectors that describe the variance in the data. The first mode of the resulting EOF is the eigenvector that describes the largest amount of the variance. The second mode is the function which describes as much of the remaining variance as possible, and so on for $n-1$ modes, where n is the number of time slices analyzed.

The result of the EOF analysis is three variables for each mode: a two-dimensional field describing the spatial pattern of variability, a dimensionless EOF index for each time slice, and the fraction of the variability for that mode. In general, each time slice is described by taking the mean spatial pattern of a given field (e.g., concentration of trajectories), and adding the spatial pattern for each EOF mode multiplied by the respective EOF index for that time slice.

For instance, for some spatial variable X, which is recorded at t points in time, we can calculate $t-1$ EOF modes. Then, we can write

$$X(t) = \langle X \rangle + \Sigma\, \mathrm{EOF}_n \times \mathrm{index}_n(t)$$

where $\langle X \rangle$ is the mean value of X over all t and EOF_n and index_n are the spatial fields and EOF indices for each EOF mode. As the EOF procedure is designed to capture as much of the variance as possible in the first few modes, the EOF modes for higher n can be neglected: in all the cases where EOF analysis was deployed here, the first mode was sufficient to describe the majority of the variability.

As well as applying this technique to the concentrations derived from our Lagrangian experiments to highlight how the advective pathways have changed, EOF analysis is applied to SSH and mixed layer depth (MLD) fields output from the annual model means. This is done to explain the reasons for the shift in advective pathways, and to explore potential consequences linked to that change in advection.

3. Results and Discussion

3.1. Variability of Sources of Beaufort Gyre Water

We begin by analyzing the sources of Beaufort Gyre freshwater, and their variability, both temporally and by depth. We start by considering all particles launched in a given year at each depth level. Figure 2 shows a stacked bar chart for each of the release depths, displaying how many particles we attributed to each source (or none at all) for each year:

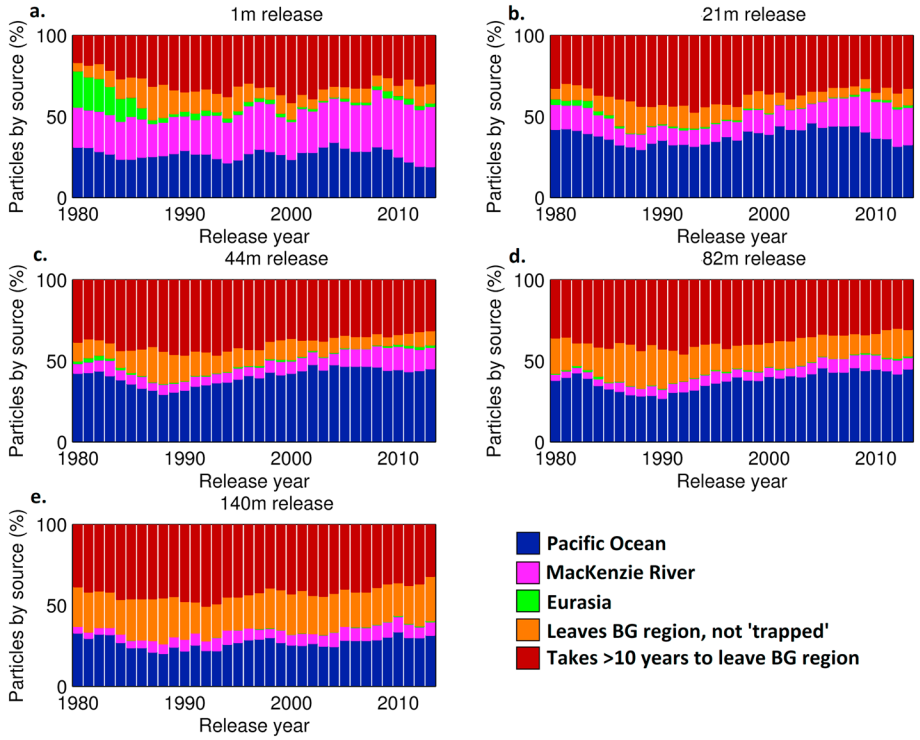

Figure 2. Relative importance of each source to the Beaufort Gyre region after 10 years of backtracking, for the period 1980–2013. Dark blue = Pacific, magenta = Mackenzie River, green = Eurasian shelf, red = did not leave BG region, orange = left BG region, but uncategorized. This is shown for each of the five depth levels studied: (a) surface releases, (b) 21-m releases, (2) 44-m releases, (d) 82-m releases, and (2) 140-m releases.

In Figure 2, the years along the *x* axis correspond to the years in which particles were initially released. Due both to the advective time scales required to go back from the gyre to one of our three sources, and the fact that particles can persist in the gyre for many years (in many cases, for the full 10 years they are tracked for—see the red bars) the year that each particle was released does not directly equate to the year in which it entered the Beaufort Gyre.

From Figure 2, it is clear that Pacific Ocean (dark blue) is the dominant source of particles in all years. 34% of all trajectories are tracked back to the Pacific Ocean, and the Pacific dominates most strongly (41% of all trajectories) for releases at 44-m depth, which is in the Pacific layer of the Beaufort Gyre. We note the trend of the Pacific contribution increasing from the late 1980s and throughout the 1990s, which is especially prominent in the 44- and 82-m releases. However, it is important to note that this does not necessarily imply that it is the dominant source of freshwater to the Beaufort Gyre—each particle backtracked to the Pacific Ocean represents a much smaller freshwater contribution than a particle backtracked to the Mackenzie River. From observations (Woodgate, 2018), it is known that the freshwater discharge from the Bering Strait (2,000–3,000 km^3/year) is an order of magnitude larger than the discharge from the Mackenzie River (300 km^3/year), which is in agreement with our experiment results showing that the majority of trajectories can be traced back to the Bering Strait.

Given that particles traced back to Pacific Ocean must have passed over the Chukchi Plateau, which is only approximately 50 m deep, and that particles initially seeded at the 82- and 140-m depth levels were found to come from the Pacific, the question of how they reached those depths are inevitably raised. As they circulate backward around the Beaufort Gyre, they were found to spiral up to shallower layers as they were backtracked to the Pacific. This corresponds to Pacific Water being pumped to these greater depths via the helical circulation pathways, as described in an idealized case by Timmermans et al. (2014).

The contribution of the Mackenzie River is more important at the surface of the Beaufort Gyre region relative to the Mackenzie contribution at greater depths. Twenty-seven percent of trajectories from the 1-m release are tracked to the Mackenzie River; however, this diminishes in importance in the deeper layers

(14%, 8%, 6%, and 7% for 21-, 44-, 82-, and 140-m releases, respectively). In contrast, the contribution of Eurasian shelf waters—including inputs from Eurasian rivers—is negligible in all layers in almost all years investigated (1.6% of all trajectories), aside from a contribution to the surface layer in the early 1980s. Due to the small, typically negligible number of particles reaching the Siberian shelf, we do not attempt to consider the relative contribution of the Siberian rivers but acknowledge this as a potential avenue for future research.

The red and orange bars in Figure 2 correspond to those particles which either never leave the gyre (red) or leave but have not yet reached another box (orange).

To summarize, the two main results that we can glean from this analysis of sources of Lagrangian particles are as follows:

1. The Beaufort Gyre is strongly layered by advective source. The vertical structure of the Beaufort Gyre region is well described (Davis et al., 2016; Lique et al., 2014; Steele et al., 2004) with a fresh upper layer above the Pacific halocline and finally the Atlantic layer at the bottom. This structure is apparent in Figure 2, with the majority of Mackenzie and Eurasian particles in the surface release, Pacific particles dominating the 44- and 82-m releases (41% and 40%, respectively), and a marked decline in Pacific particles from the 140-m release (27%), which corresponds approximately to the base of the Pacific layer in the Canada Basin (Steele et al., 2004).
2. The contribution of Pacific water to the Beaufort Gyre has increased since the late 1980s. This trend is most obvious in the 44- and 82-m layers, where the Pacific contribution increased by 43% in these layers between 1988 and 2000. This trend is in agreement with observations which have noted an increase in Pacific inflow to the Arctic via the Bering Strait over the same period (Woodgate, 2018).

3.2. Changing Pathways: The Waiting Room

To investigate how the circulation pathways have changed between the 1980s and present day, we focused on the contribution from the Pacific Ocean using only the subset of trajectories that crossed the Bering Strait. To get around the problem of particles remaining in the Beaufort Gyre for several years before eventually leaving, we recategorized them based on the year in which they crossed the Bering Strait rather than the time of their initial release. Particles tracked to other sources (or none) are disregarded in this analysis. As particles were released every year between 1980 and 2013 before being backtracked for 10 years, Bering Strait crossings occur every year from 1970 to 2013. To avoid biasing the results with under sampled years (e.g., crossing in 1971 are only possible from the 1980 or 1981 releases, and in 2012 only from the 2012 or 2013 experiments), only particles which crossed the Bering Strait between 1980 and 2003 are considered.

Considering only these particles, we divided the Arctic into a 1° (longitude) × 0.5° (latitude) grid (to make approximately square 3,000-km^2 grid cells in the Beaufort Gyre region) and calculated the density of trajectories passing through each cell, weighted by area of each grid cell. These densities were calculated for each year (by Bering Strait crossing) 1980–2003, and an empirical orthogonal function (full description in section 2.3) analysis was performed to characterize the variability of the particles' trajectories.

Figure 3a shows the first mode characterizing 65.3% of variability of the trajectory densities: blues (in both the Beaufort Gyre region and the Pacific Ocean) being negative and reds positive. The interpretation of this map and the indices shown in Figure 3b is that in years with positive indices, more trajectories pass through the red regions and fewer through the blue. Years with negative indices correspond to an above average number of trajectories in the blue regions of Figure 3a, but a decrease in the red regions.

The indices for this mode (Figure 3b) go from positive in the 1980s to "increasingly" negative throughout the 1990s. As both the Pacific Ocean and Beaufort Gyre region are shown blue in Figure 3a, this implies that the Pacific contribution to the Beaufort Gyre in our experiments was reduced in years with positive indices, and increased in years with negative indices. As the indices in Figure 3b go from positive to negative from the 1980s to the 1990s, this suggests that Pacific contribution to the Gyre did indeed increase throughout the 1980s and 1990s, in agreement with the trajectory analysis presented in Figure 2.

More interestingly, we see that the increase in Pacific contribution to the Beaufort Gyre also correlated with a change in circulation in the Arctic Ocean: this can be identified from the red region in Figure 3a. An increase in particles flowing through this area is out of phase with both particles in the Pacific Ocean and in the Beaufort Gyre.

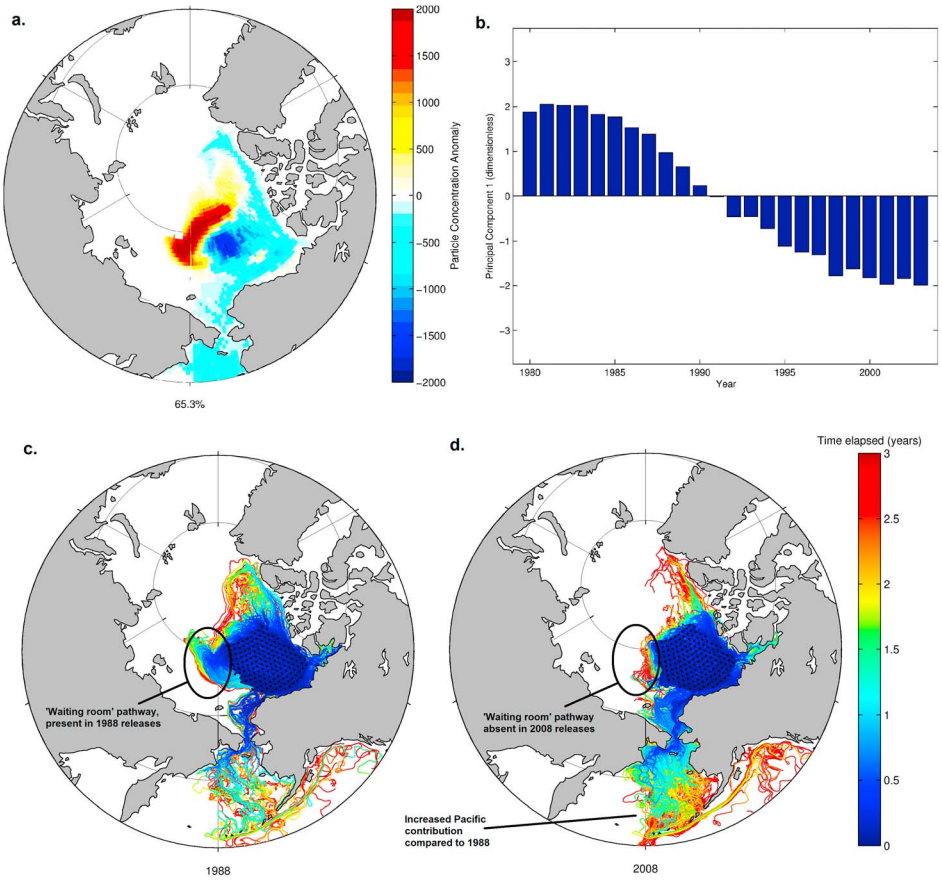

Figure 3. (a) Spatial pattern of first mode of EOF analysis of trajectory densities for particles tracked back to the Pacific Ocean. (b) EOF indices for the first EOF mode. Note that here we classify particles based on the year they crossed the Bering Strait, regardless of when they were initialized. This mode describes 65.3% of the variability of Pacific inflow to the Beaufort Gyre. Years with positive indices correspond to more trajectories flowing through the red regions in (a), and fewer through the blue. Vice versa is true for years with negative indices. (c) Comparison of the first three years of Lagrangian trajectories backtracked from 1988 (waiting room) and (d) 2008 (no waiting room), respectively. Color of trajectories denotes the time that each particle has been backtracked for.

The interpretation of this is as follows: when the dominant Arctic circulation is less favorable for water to accumulate into the Beaufort Gyre, the water that does come through the Bering Strait is directed into this red region. This contrasts with the years with a favorable circulation, in which Pacific Water is permitted to flow directly into the Beaufort Gyre itself. We term this red area the "waiting room," as it represents a prolonged pathway by which Pacific Water flows to the Beaufort Gyre in years when Pacific Water is less readily able to make it to the gyre. This waiting room is the dominant feature, accounting for the majority (65.3%) of the differences between the years studied. As Figure 3b shows, this feature has diminished in importance throughout our experiments, and suggests a secular trend whereby this pathway is no longer available in a changed Arctic Ocean.

This is further illustrated in Figures 3c and 3d, where an example of a favorable year for Pacific Water entering the gyre (2008 release) is compared to an unfavorable year (1988 release). In this case, only the first three years of backtracking are shown, with colors of trajectories denoting how much backtracking time has elapsed since each particle was released. Blues are plotted on top of reds. The waiting room, present in the 1988 release but not in 2008, is clearly visible.

3.3. Cause of the Waiting Room

To investigate the dynamics of favorable/unfavorable years for Pacific Water entering the Beaufort Gyre, and to validate the model results, Ekman transport was calculated based on observed wind, ice concentration, ice motion, and geostrophic currents. This was done for the years with the most positive (1983–1985) and most

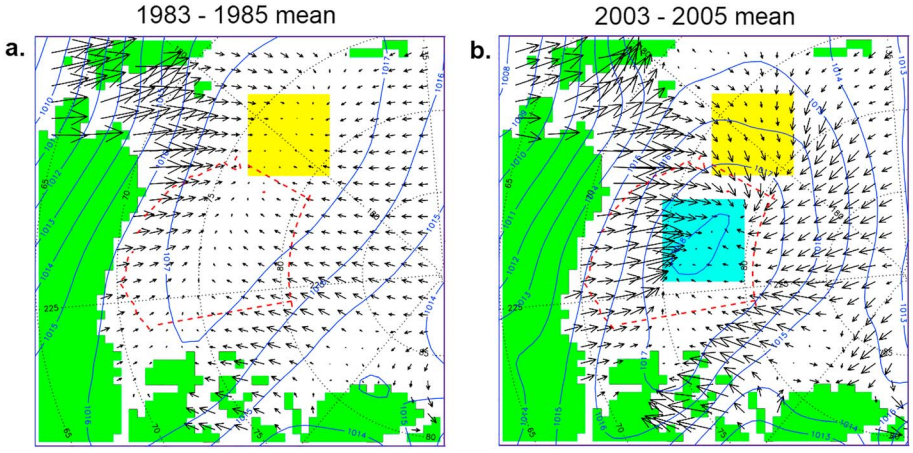

Figure 4. Ekman transport for the periods (a) 1983–1985 and (b) 2003–2005. Blue lines indicate sea level pressure, red dashed line represents the Beaufort Gyre region, and land is shown in green. The waiting room region is highlighted in yellow. Note that this is where the Ekman transport converges in 1983–1985. The cyan region shows the center of Ekman convergence for 2003–2005. Unlike in 1983–1985, this is within the Beaufort Gyre region for the 2003–2005 period.

negative (2003–2005) EOF indices, corresponding to least and most favorable for Pacific Water accumulation in our Lagrangian experiments. This is presented in Figure 4. External forcing factors accounted for calculations of Ekman transport include geostrophic wind velocities, sea ice concentration and drift, and oceanic geostrophic velocities, all calculated using established methods. Ekman transports are determined following the methods of Meneghello et al. (2017) and Meneghello et al. (2018) and are identical to the approach published by Regan et al. (2019) in this special issue. The geostrophic wind was calculated from National Center for Atmospheric Research/National Centers for Environmental Prediction (reanalysis 1; Cavalieri et al., 1996) 6-hourly sea level pressure (SLP) fields. Sea ice motion is taken from the Polar Pathfinder Daily 25 km EASE-Grid Sea Ice Motion Vectors, version 4 (Tschudi et al., 2019). Daily sea ice concentration for 2003–2018 is from Nimbus-7 SMMR and DMSP SSM/I-SSMIS Passive Microwave Data version 1 (Cavalieri et al., 1996). The ocean geostrophic velocity fields are from Armitage et al. (2017).

In 1983–1985 (Figure 4a), the Ekman transport converged in the waiting room region (yellow box) and hence particles accumulated there. This observational evidence provides supports for the suggestion from Figure 3 that 1983–1985 wind forcing (inferred from sea level pressure, hereafter referred to as SLP) was favorable for accumulation of particles in the waiting room but unfavorable for freshwater accumulation in the Beaufort Gyre region.

In 2003–2005 (Figure 4b), the wind pattern was different. The center of high SLP shifted toward the center of the Beaufort Gyre, and Ekman transport convergence was also in the Beaufort Gyre's center (cyan box). This SLP and wind pattern was favorable for accumulation of freshwater (particles) into the Beaufort Gyre region. In Figure 4b, it is also apparent that Ekman transport was responsible for bringing particles from the waiting room to the Beaufort Gyre center.

The size and shape of the Beaufort Gyre depends on the strength and location of the SLP maximum (Beaufort High). Analysis of the observed spatial extent and shape of the Beaufort Gyre (Regan et al., 2019) showed a north-westward shift of the Beaufort Gyre center and hence an expansion of the Beaufort Gyre between 2003 and 2014. Regan et al. (2019) noted that SLP maxima to the west of the gyre (as in Figure 4b here) lead to an enlargement of the western extent of the Beaufort Gyre, into the waiting room region identified here. We suggest that the advective pathways identified in Figure 3 are a consequence of Pacific Water becoming entrained in the Beaufort Gyre in this waiting room region outside of the gyre's usual extent due to a wind-forced expansion of the Beaufort Gyre. Pacific Water first passes through this region (hence the term waiting room) before entering the main Beaufort Gyre region.

As has already been established previously (e.g., Giles et al., 2012; Polyakov et al., 1999; Proshutinsky et al., 1999) wind forcing is the primary driver of the Beaufort Gyre, and the Arctic Ocean Oscillation—which describes the ocean's response to the atmospheric forcing—explains the net accumulation or release of

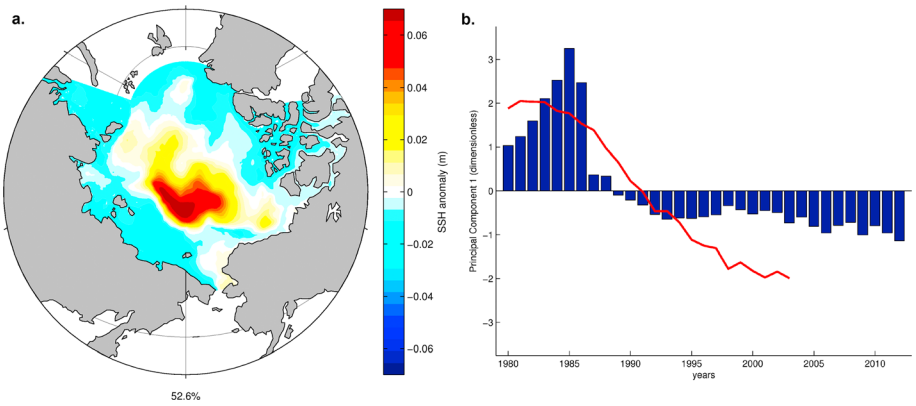

Figure 5. First mode of EOF analysis of sea surface height across the Arctic Ocean. This mode describes 52.6% of the variability. A raised area that approximately corresponds to the "waiting room" region identified in section 3.2 is apparent and varies on a time scale that correlates ($r = 0.83$) with the EOF indices calculated in Figure 3. The indices from Figure 3b (from 1980 to 2003) are replotted as a red line in Figure 5b.

freshwater. This response manifests itself as a barotropic change in sea surface height (see Proshutinsky and Johnson (1997) and Proshutinsky et al. (2015) for full details of the Arctic Ocean Oscillation index).

Balancing this wind-driven accumulation of freshwater, eddies play a key role in bringing waters away from the shelf break currents (Spall et al., 2008) and the Beaufort Gyre, constraining the maximum freshwater content in the region (Manucharyan & Spall, 2016). Observations have demonstrated that this is indeed happening, with ice-tethered profilers recording an increase in eddy density over the period 2005–2015, in response to more baroclinic instabilities which balance the input of wind energy in the Beaufort Gyre region (Zhao et al., 2016). This is in agreement with idealized model studies, which demonstrate that the intensity of the Arctic surface circulation is set by the balance between Ekman pumping and eddy-driven transport toward the boundary over a decadal time scale (Lique et al., 2015).

With NEMO, we are able to consider both barotropic and baroclinic effects. Changes in sea surface height in the Arctic are a function of wind forcing, as reflected by the AOO (Proshutinsky & Johnson, 1997). We compared the modeled annual mean SSH fields on a pan-Arctic scale as a proxy for the ocean's response to wind forcing and, as with the trajectory densities, we performed empirical orthogonal function analysis to extract the trend in SSH over the years studied. The EOF analysis was performed over the domain north of 66°N, excluding 80°W to 70°E to avoid considering Atlantic waters away from the vicinity of gyre. (The same domain is also used in Figure 6, for the same reasons.) The result of this analysis is presented in Figure 5.

From the first mode of EOF map in Figure 5, it is apparent that the majority (52.6%) of the variability in sea surface height is explained by a feature centered toward the Eurasian side of the Beaufort Gyre which largely coincides with the waiting room region identified from Lagrangian trajectories. The EOF indices (blue bars) show that this region was raised relative to the 1980–2013 mean throughout the 1980s, and shallower from the 1990s onward.

The timing of this correlates ($r = 0.83$) with the appearance/disappearance of the waiting room pathway identified in section 3.2. The first mode of EOF indices calculated in Figure 3 is replotted as the red line in Figure 5 to highlight this.

The fact that the change in circulation evidenced by the Lagrangian trajectories can be explained by changes in sea surface height suggests that the "waiting room pathway" is primarily a consequence of a change in the surface circulation rather than a shift in deeper currents. Given that the Arctic has changed rapidly in recent decades—warming, and with reduced sea ice to mediate the effect of the wind on the ocean surface—we suggest that this change in circulation is a secular trend rather than a consequence of known variability (e.g., the Arctic Ocean Oscillation.) However, it is worth noting that the AOO remained positive for 20 years after 1997, rather than its previous 5–7 years in either mode.

Previous work (Kelly et al., 2018) has shown that this configuration of NEMO does a good job of representing observed (Armitage et al., 2016) sea surface height, and additional validation (see supporting information)

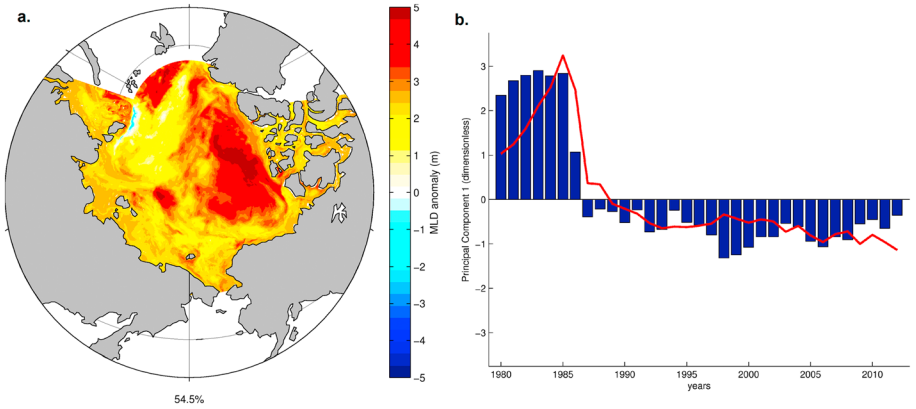

Figure 6. First mode of EOF mixed layer depth in the Arctic Ocean. Blue bars show EOF indices for this mode, and red line replots the indices from Figure 5 for sake of comparison. This mode describes 54.5% of the variability in the region shown and shows a shoaling of the Arctic mixed layer depth since the mid-1980s, with this effect most pronounced in the Canada Basin. The time scale of this variability correlates ($r = 0.89$) with the indices in Figure 5b and replotted as the red line here.

shows that for the Envisat observational period, the main nonseasonal mode of variability is comparable in both model and observations.

3.4. Implications of the Waiting Room

Having presented evidence that changes in the surface circulation switched off the modeled waiting room advective pathway between the 1980s and early 2010s, we now discuss why this is important for the Arctic in general.

Using the same EOF technique as previously, we investigated how the modeled MLD throughout the Arctic Ocean changed between 1980 and 2013. The mixed layer depth used here was calculated based on a density criterion (De Boyer Montégut et al., 2004), where the potential density differs by 0.01 kg/m^3 relative to a reference density at 10-m depth.

There is observational evidence that in recent decades, the mixed layer depth throughout the Arctic has shoaled as the Arctic has freshened (Peralta-Ferriz & Woodgate, 2015). This result is reflected in the model simulation underlying this work, and we also find that this is not uniform over the Arctic. Rather, the shoaling has been especially pronounced in the Beaufort Gyre region and the Canada Basin (Figure 6). However, it is worth noting that the observations note one exception: a deepening of the mixed layer in the Southern Beaufort Sea between 1979 and 2012 (Peralta-Ferriz & Woodgate, 2015), which does not feature in our model result—although the modeled shoaling in the Southern Barents Sea is markedly lower than in the Canada Basin itself.

Interestingly, the change in mixed layer depth correlates very strongly ($r = 0.89$) with the change in sea surface height from Figure 5. We propose that the change in circulation, which led to an increase in Pacific contribution to the Beaufort Gyre, may have played a role in this amplified shoaling of the mixed layer depth in the Beaufort Gyre region.

The Beaufort Gyre region is strongly stratified, with a fresh upper mixed layer above the Pacific halocline, in turn-on top of the Atlantic halocline and Arctic bottom water. We argue that the disappearance of the waiting room pathway since the 1980s, as evidenced by Lagrangian trajectories and Ekman transports derived from observations, allowed more Pacific water to directly enter the Beaufort Gyre. Furthermore, we note that this increased Pacific contribution coincided with a shoaling of the mixed layer in the Beaufort Gyre region. Given the strong correlation between the shift in circulation and shoaling of Beaufort Gyre mixed layer depth, we hypothesize that the change in advective pathways may have contributed to explaining why the MLD in the Beaufort Gyre changed more than the rest of the Arctic. Further analysis is required to investigate the link between the Pacific layer of the Beaufort Gyre and the MLD in the region.

It is important to note that this is not the only factor at play: sea ice has declined rapidly over recent decades, and this has feedback which directly affect Arctic mixing. For instance, this causes freshening of the surface of the ocean, which in turn strengthens the stratification and therefore works to shoal the mixed layer. Nevertheless, melting of sea ice means more open water for longer, and therefore an increase in wind-driven mixing across the Arctic Ocean. We note that these effects, along with the changed circulation, are all involved in governing the mixed layer in the Arctic Ocean. Additional experiments are required to ascertain the relative importance of different contributing factors.

The shoaling of Beaufort Gyre mixed layer depth suggested by NEMO is potentially important not just for the mixing in the Beaufort Gyre region but also for the biology of the Arctic. The biogeochemistry is governed in part by the stratification (e.g., Popova et al., 2010)—weaker stratification and increased mixing enables more nutrients to be brought to the surface which improves growing conditions for phytoplankton and can potentially increase marine productivity. Meanwhile, a more strongly stratified ocean inhibits mixing and can place a limit on the availability of nutrients and hence on the biological activity in the Arctic.

The link between changed advective pathways and shoaled MLD is of particular interest, as an increased Pacific contribution to the gyre naturally means an increase in Pacific biomass entering the region (Wassmann et al., 2015). With climate change induced shifts in Arctic circulation hypothesized as a potential explanation for "invasions" of nonnative species (Reid et al., 2007), the potential link between changed circulation pathways and the hospitability of the ocean is important for assessing the viability of these "invasion" hypotheses.

4. Summary and Conclusions

Based on our analysis and experiments described above, we note and hypothesize the following:

1. Between 1980 and 2000, our analysis finds that the Pacific contribution of freshwater to the Beaufort Gyre increased;
2. This increase coincided with a change in atmospheric and sea ice and ocean circulation that more directly supplies Pacific freshwater to the Beaufort Gyre instead of using a longer advective pathway, the waiting room;
3. Analysis attributes the change in circulation to a shift in prevailing wind patterns, as evidenced by a change in sea surface height that correlates with the changed circulation pathways. Further analysis demonstrated that this change was caused by a shift in the center of Ekman convergence from the waiting room region in the 1980s to the Beaufort Gyre region from the 1990s onward;
4. In turn, shoaling mixed layer depths in the Beaufort Gyre correlate with this changing circulation, and this change is much stronger than the increasing stratification across the wider Arctic;
5. Our analysis supports the conjecture that the changes in circulation are responsible for the increased Beaufort Gyre stratification, mediated by the enhanced freshwater supply;
6. Because of the critical role of stratification for marine productivity, as well as the role of Pacific inflow waters in supplying nutrients, we speculate that these changes potentially have wider impacts for Arctic ecology.
7. Further modeling experiments and analysis of observational data are needed to test these hypotheses.
8. We note that this research is limited in that while it can help to describe changes in the Pacific contribution to the Beaufort Gyre, it cannot address the freshwater contribution to the Beaufort Gyre from meltwater or precipitation, and that the contribution from the Mackenzie River is only approximated by tracking particles back to the vicinity of the its plume.
9. Additionally, we are constrained by only using the NEMO model and ARIANE particle tracking package. Intercomparison work, using different models and different particle tracking software, would be useful to validate the results presented in this paper.
10. Further work could focus on the Siberian contribution to the Beaufort Gyre. Due to the small number of particles tracked back to the Siberian shelf, a thorough analysis of the contribution (or lack thereof) of Siberian river water to the Beaufort Gyre would be an interesting avenue for future research. A Lagrangian forward-tracking approach, following particles seeded at the mouths of these rivers, could contribute to this work.

Acknowledgments

The underpinning high-resolution NEMO simulation was performed using the ARCHER UK National Supercomputing Service (http://www.archer.ac.uk). ARIANE simulations were performed using the JASMIN data analysis environment (http://www.jasmin.ac.uk). Lagrangian analysis was carried out using computational tool ARIANE developed by B. Blanke and N. Grima. Arctic dynamic topography/geostrophic currents data were provided by the Centre for Polar Observation and Modelling, University College London (www.cpom.ucl.ac.uk/dynamic_topography; Armitage et al., 2016). The funding for A. Proshutinsky was provided by the NSF under grants supporting the Beaufort Gyre Observing System since 2003 (1845877, 1719280, 1604085) and by the Woods Hole Oceanographic Institution. Y. Aksenov was supported from the NERC Program "The North Atlantic Climate System Integrated Study (ACSIS), NE/N018044/1 and from the project "Advective pathways of nutrients and key ecological substances in the Arctic (APEAR)" NE/R012865/1, as a part of the joint UK/Germany "Changing Arctic Ocean" Programme. A. Yool and E. Popova were supported by NERC grants CLASS NE/R015953/1, and National Capability in Ocean Modelling. We acknowledge the FAMOS (http://web.whoi.edu/famos/) program for providing a framework for many fruitful discussions which thoroughly enhanced this work. Finally, we thank the two anonymous reviewers who greatly improved this work with their insightful input.

References

Aagaard, K., & Carmack, E. C. (1989). The role of sea ice and other fresh water in the Arctic circulation. *Journal of Geophysical Research*, *94*(C10), 14,485–14,498. https://doi.org/10.1029/JC094iC10p14485

Aksenov, Y., Karcher, M., Proshutinsky, A., Gerdes, R., De Cuevas, B., Golubeva, E., et al. (2016). Arctic pathways of Pacific Water: Arctic Ocean Model Intercomparison experiments. *Journal of Geophysical Research: Oceans*, *121*, 27–59. https://doi.org/10.1002/2015JC011299

Aksenov, Y., Popova, E. E., Yool, A., Nurser, A. J. G., Williams, T. D., Bertino, L., & Bergh, J. (2017). On the future navigability of Arctic sea routes: High-resolution projections of the Arctic Ocean and sea ice. *Marine Policy*, *75*, 300–317. https://doi.org/10.1016/j.marpol.2015.12.027

Alkire, M. B., Morison, J., Schweiger, A., Zhang, J., Steele, M., Peralta-Ferriz, C., & Dickinson, S. (2017). A meteoric water budget for the Arctic Ocean. *Journal of Geophysical Research: Oceans*, *122*, 10,020–10,041. https://doi.org/10.1002/2017JC012807

Armitage, T. W. K., Bacon, S., Ridout, A. L., Petty, A. A., Wolbach, S., & Tsamados, M. (2017). Arctic Ocean surface geostrophic circulation 2003–2014. *The Cryosphere*, *11*(4), 1767–1780. https://doi.org/10.5194/tc-11-1767-2017

Armitage, T. W. K., Bacon, S., Ridout, A. L., Thomas, S. F., Aksenov, Y., & Wingham, D. J. (2016). Arctic sea surface height variability and change from satellite radar altimetry and GRACE, 2003–2014. *Journal of Geophysical Research: Oceans*, *121*, 4303–4322. https://doi.org/10.1002/2015JC011579

Blanke, B., & Raynaud, S. (1997). Kinematics of the Pacific Equatorial Undercurrent: An Eulerian and Lagrangian approach from GCM results. *Journal of Physical Oceanography*, *27*(6), 1038–1053. https://doi.org/10.1175/1520-0485(1997)027<1038:KOTPEU>2.0.CO;2

Boe, J., Hall, A., & Qu, X. (2009). September sea-ice cover in the Arctic Ocean projected to vanish by 2100. *Nature Geoscience*, *2*(5), 341–343. https://doi.org/10.1038/ngeo467

Brodeau, L., Barnier, B., Treguier, A.-M., Penduff, T., & Gulev, S. (2010). An ERA40-based atmospheric forcing for global ocean circulation models. *Ocean Modelling*, *31*(3-4), 88–104. https://doi.org/10.1016/j.ocemod.2009.10.005

Cao, Y., Liang, S., Chen, X., He, T., Wang, D., & Cheng, X. (2017). Enhanced wintertime greenhouse effect reinforcing Arctic amplification and initial sea-ice melting. *Scientific Reports*, *7*(1), 8462. https://doi.org/10.1038/s41598-017-08545-2

Carmack, E. C., Yamamoto-Kawai, M., Haine, T. W. N., Bacon, S., Bluhm, B. A., Lique, C., et al. (2016). Freshwater and its role in the Arctic Marine System: Sources, disposition, storage, export, and physical and biogeochemical consequences in the Arctic and global oceans. *Journal of Geophysical Research: Biogeosciences*, *121*, 675–717. https://doi.org/10.1002/2015JG003140

Cavalieri, C. L. P., Gloersen, P., & Zwally, H. J. (1996). In C. L. P. Cavalieri, P. Gloersen, & H. J. Zwally (Eds.), *Sea ice concentrations from Nimbus-7 SMMR and DMSP SSM/I-SSMIS Passive Microwave Data, version 1*. Boulder, Colorado USA: NASA National Snow and Ice Data Center Distributed Active Archive Center.

Cohen, J., Screen, J. A., Furtado, J. C., Barlow, M., Whittleston, D., Coumou, D., et al. (2014). Recent Arctic amplification and extreme mid-latitude weather. *Nature Geoscience*, *7*(9), 627–637. https://doi.org/10.1038/ngeo2234

Davis, P. E. D., Lique, C., Johnson, H. L., & Guthrie, J. D. (2016). Competing effects of elevated vertical mixing and increased freshwater input on the stratification and sea ice cover in a changing Arctic Ocean. *Journal of Physical Oceanography*, *46*(5), 1531–1553. https://doi.org/10.1175/JPO-D-15-0174.1

De Boyer Montégut, C., Madec, G., Fischer, A. S., Lazar, A., & Iudicone, D. (2004). Mixed layer depth over the global ocean: An examination of profile data and a profile-based climatology. *Journal of Geophysical Research*, *109*, C12003. https://doi.org/10.1029/2004JC002378

Fichefet, T., & Maqueda, M. A. M. (1997). Sensitivity of a global sea ice model to the treatment of ice thermodynamics and dynamics. *Journal of Geophysical Research*, *102*(C6), 12,609–12,646. https://doi.org/10.1029/97JC00480

Giles, K. A., Laxon, S. W., Ridout, A. L., Wingham, D. J., & Bacon, S. (2012). Western Arctic Ocean freshwater storage increased by wind-driven spin-up of the Beaufort Gyre. *Nature Geoscience*, *5*(3), 194–197. https://doi.org/10.1038/ngeo1379

Goosse, H., & Fichefet, T. (1999). Importance of ice-ocean interactions for the global ocean circulation: A model study. *Journal of Geophysical Research*, *104*(C10), 23,337–23,355. https://doi.org/10.1029/1999JC900215

Graversen, R. G., Mauritsen, T., Tjernström, M., Källén, E., & Svensson, G. (2008). Vertical structure of recent Arctic warming. *Nature*, *451*(7174), 53–56. https://doi.org/10.1038/nature06502

Hu, X., & Myers, P. G. (2013). A Lagrangian view of Pacific water inflow pathways in the Arctic Ocean during model spin-up. *Ocean Modelling*, *71*, 66–80. https://doi.org/10.1016/j.ocemod.2013.06.007

Janout, M. A., Aksenov, Y., Hölemann, J. A., Rabe, B., Schauer, U., Polyakov, I. V., et al. (2015). Kara Sea freshwater transport through Vilkitsky Strait: Variability, forcing, and further pathways toward the western Arctic Ocean from a model and observations. *Journal of Geophysical Research: Oceans*, *120*, 4925–4944. https://doi.org/10.1002/2014JC010635

Karcher, M., Smith, J. N., Kauker, F., Gerdes, R., & Smethie, W. M. Jr. (2012). Recent changes in Arctic Ocean circulation revealed by iodine-129 observations and modeling. *Journal of Geophysical Research*, *117*, C08007. https://doi.org/10.1029/2011JC007513

Kelly, S., Popova, E., Aksenov, Y., Marsh, R., & Yool, A. (2018). Lagrangian modeling of Arctic Ocean circulation pathways: Impact of advection on spread of pollutants. *Journal of Geophysical Research: Oceans*, *123*, 2882–2902. https://doi.org/10.1002/2017JC013460

Krishfield, R. A., Proshutinsky, A., Tateyama, K., Williams, W. J., Carmack, E. C., Mclaughlin, F. A., & Timmermans, M.-L. (2014). Deterioration of perennial sea ice in the Beaufort Gyre from 2003 to 2012 and its impact on the oceanic freshwater cycle. *Journal of Geophysical Research: Oceans*, *119*, 1271–1305. https://doi.org/10.1002/2013JC008999

Lique, C., Guthrie, J. D., Steele, M., Proshutinsky, A., Morison, J. H., & Krishfield, R. (2014). Diffusive vertical heat flux in the Canada Basin of the Arctic Ocean inferred from moored instruments. *Journal of Geophysical Research: Oceans*, *119*, 496–508. https://doi.org/10.1002/2013JC009346

Lique, C., Johnson, H. L., & Davis, P. E. D. (2015). On the Interplay between the circulation in the surface and the intermediate layers of the Arctic Ocean. *Journal of Physical Oceanography*, *45*(5), 1393–1409. https://doi.org/10.1175/JPO-D-14-0183.1

Lique, C., Treguier, A. M., Blanke, B., & Grima, N. (2010). On the origins of water masses exported along both sides of Greenland: A Lagrangian model analysis. *Journal of Geophysical Research*, *115*, C05019. https://doi.org/10.1029/2009JC005316

Luneva, M. V., Aksenov, Y., Harle, J. D., & Holt, J. T. (2015). The effects of tides on the water mass mixing and sea ice in the Arctic Ocean. *Journal of Geophysical Research: Oceans*, *120*, 6669–6699. https://doi.org/10.1002/2014JC010310

Madec, G. 2014. "NEMO ocean engine" (Draft edition r5171). Note du Pôle de modélisation, Institut Pierre-Simon Laplace (IPSL), France, No 27 ISSN No 1288–1619.

Manucharyan, G. E., & Spall, M. A. (2016). Wind-driven freshwater buildup and release in the Beaufort Gyre constrained by mesoscale eddies. *Geophysical Research Letters*, *43*, 273–282. https://doi.org/10.1002/2015GL065957

Mcphee, M. G., Proshutinsky, A., Morison, J. H., Steele, M., & Alkire, M. B. (2009). Rapid change in freshwater content of the Arctic Ocean. *Geophysical Research Letters*, *36*, L10602. https://doi.org/10.1029/2009GL037525

Meneghello, G., Marshall, J., Campin, J.-M., Doddridge, E., & Timmermans, M.-L. (2018). The ice-ocean governor: Ice-ocean stress feedback limits Beaufort Gyre spin-up. *Geophysical Research Letters*, *45*, 11,293–11,299. https://doi.org/10.1029/2018GL080171

Meneghello, G., Marshall, J., Cole, S. T., & Timmermans, M.-L. (2017). Observational inferences of lateral eddy diffusivity in the halocline of the Beaufort Gyre. *Geophysical Research Letters*, *44*, 12,331–12,338. https://doi.org/10.1002/2017GL075126

Nurser, A. J. G., & Bacon, S. (2014). The Rossby radius in the Arctic Ocean. *Ocean Science*, *10*(6), 967–975. https://doi.org/10.5194/os-10-967-2014

Overland, J. E., & Wang, M. (2013). When will the summer Arctic be nearly sea ice free? *Geophysical Research Letters*, *40*, 2097–2101. https://doi.org/10.1002/grl.50316

Peralta-Ferriz, C., & Woodgate, R. A. (2015). Seasonal and interannual variability of pan-Arctic surface mixed layer properties from 1979 to 2012 from hydrographic data, and the dominance of stratification for multiyear mixed layer depth shoaling. *Progress in Oceanography*, *134*, 19–53. https://doi.org/10.1016/j.pocean.2014.12.005

Polyakov, I. V., Pnyushkov, A. V., Alkire, M. B., Ashik, I. M., Baumann, T. M., Carmack, E. C., et al. (2017). Greater role for Atlantic inflows on sea-ice loss in the Eurasian Basin of the Arctic Ocean. *Science*, *356*(6335), 285–291. https://doi.org/10.1126/science.aai8204

Polyakov, I. V., Proshutinsky, A. Y., & Johnson, M. A. (1999). Seasonal cycles in two regimes of Arctic climate. *Journal of Geophysical Research*, *104*(C11), 25,761–25,788. https://doi.org/10.1029/1999JC900208

Polyakov, I. V., Timokhov, L. A., Alexeev, V. A., Bacon, S., Dmitrenko, I. A., Fortier, L., et al. (2010). Arctic Ocean warming contributes to reduced polar ice cap. *Journal of Physical Oceanography*, *40*(12), 2743–2756. https://doi.org/10.1175/2010JPO4339.1

Popova, E. E., Yool, A., Aksenov, Y., & Coward, A. C. (2013). Role of advection in Arctic Ocean lower trophic dynamics: A modeling perspective. *Journal of Geophysical Research: Oceans*, *118*, 1571–1586. https://doi.org/10.1002/jgrc.20126

Popova, E. E., Yool, A., Coward, A. C., Aksenov, Y. K., Alderson, S. G., de Cuevas, B. A., & Anderson, T. R. (2010). Control of primary production in the Arctic by nutrients and light: insights from a high resolution ocean general circulation model. *Biogeosciences*, *7*, 3569–3591. https://doi.org/10.5194/bg-7-3569-2010

Proshutinsky, A., Bourke, R. H., & Mclaughlin, F. A. (2002). The role of the Beaufort Gyre in Arctic climate variability: Seasonal to decadal climate scales. *Geophysical Research Letters*, *29*(23), 2100. https://doi.org/10.1029/2002GL015847

Proshutinsky, A., Dukhovskoy, D., Timmermans, M.-L., Krishfield, R., & Bamber, J. L. (2015). Arctic circulation regimes. *Philosophical Transactions of the Royal Society A: Mathematical, Physical and Engineering Sciences*, *373*(2052). https://doi.org/10.1098/rsta.2014.0160

Proshutinsky, A., Krishfield, R., Timmermans, M.-L., Toole, J., Carmack, E., Mclaughlin, F., et al. (2009). Beaufort Gyre freshwater reservoir: State and variability from observations. *Journal of Geophysical Research*, *114*, C00A10. https://doi.org/10.1029/2008JC005104

Proshutinsky, A. Y., & Johnson, M. A. (1997). Two circulation regimes of the wind-driven Arctic Ocean. *Journal of Geophysical Research*, *102*(C6), 12,493–12,514. https://doi.org/10.1029/97JC00738

Proshutinsky, A. Y., Polyakov, I. V., & Johnson, M. A. (1999). Climate states and variability of Arctic ice and water dynamics during 1946–1997. *Polar Research*, *18*, 135–142.

Rabe, B., Karcher, M., Kauker, F., Schauer, U., Toole, J. M., Krishfield, R. A., et al. (2014). Arctic Ocean basin liquid freshwater storage trend 1992–2012. *Geophysical Research Letters*, *41*, 961–968. https://doi.org/10.1002/2013GL058121

Regan, H. C., Lique, C., & Armitage, T. W. K. (2019). The Beaufort Gyre extent, shape, and location between 2003 and 2014 from satellite observations. *Journal of Geophysical Research: Oceans*, *124*, 844–862. https://doi.org/10.1029/2018JC014379

Reid, P. C., Johns, D. G., Edwards, M., Starr, M., Poulin, M., & Snoeijs, P. (2007). A biological consequence of reducing Arctic ice cover: Arrival of the Pacific diatom *Neodenticula seminae* in the North Atlantic for the first time in 800,000 years. *Global Change Biology*, *13*(9), 1910–1921. https://doi.org/10.1111/j.1365-2486.2007.01413.x

Rippeth, T. P., Lincoln, B. J., Lenn, Y.-D., Green, J. A. M., Sundfjord, A., & Bacon, S. (2015). Tide-mediated warming of Arctic halocline by Atlantic heat fluxes over rough topography. *Nature Geoscience*, *8*(3), 191–194. https://doi.org/10.1038/ngeo2350

Spall, M. A., Pickart, R. S., Fratantoni, P. S., & Plueddemann, A. J. (2008). Western Arctic shelfbreak eddies: Formation and transport. *Journal of Physical Oceanography*, *38*(8), 1644–1668. https://doi.org/10.1175/2007JPO3829.1

Steele, M., Morison, J., Ermold, W., Rigor, I., Ortmeyer, M., & Shimada, K. (2004). Circulation of summer Pacific halocline water in the Arctic Ocean. *Journal of Geophysical Research*, *109*, C02027. https://doi.org/10.1029/2003JC002009

Stroeve, J. C., Schroder, D., Tsamados, M., & Feltham, D. (2018). Warm winter, thin ice? *The Cryosphere*, *12*(5), 1791–1809. https://doi.org/10.5194/tc-12-1791-2018

Timmermann, R., Goosse, H., Madec, G., Fichefet, T., Ethe, C., & Dulière, V. (2005). On the representation of high latitude processes in the ORCA-LIM global coupled sea ice–ocean model. *Ocean Modelling*, *8*(1-2), 175–201. https://doi.org/10.1016/j.ocemod.2003.12.009

Timmermans, M. L., Proshutinsky, A., Golubeva, E., Jackson, J. M., Krishfield, R., Mccall, M., et al. (2014). Mechanisms of Pacific summer water variability in the Arctic's Central Canada Basin. *Journal of Geophysical Research: Oceans*, *119*, 7523–7548. https://doi.org/10.1002/2014JC010273

Tschudi, W. N. M., Stewart, J. S., Fowler, C., & Maslanik, J. (2019). *Polar Pathfinder Daily 25 km EASE-Grid Sea Ice Motion Vectors, version 4*. Boulder, Colorado USA: NASA National Snow and Ice Data Center Distributed Active Archive Center.

Wagner, P., Rühs, S., Schwarzkopf, F. U., Koszalka, I. M., & Biastoch, A. (2019). Can Lagrangian tracking simulate tracer spreading in a high-resolution ocean general circulation model? *Journal of Physical Oceanography*, *49*(5), 1141–1157. https://doi.org/10.1175/JPO-D-18-0152.1

Wang, M., & Overland, J. E. (2012). A sea ice free summer Arctic within 30 years: An update from CMIP5 models. *Geophysical Research Letters*, *39*, L18501. https://doi.org/10.1029/2012GL052868

Wang, Q., Wekerle, C., Danilov, S., Sidorenko, D., Koldunov, N., Sein, D., et al. (2019). Recent sea ice decline did not significantly increase the total liquid freshwater content of the Arctic Ocean. *Journal of Climate*, *32*(1), 15–32. https://doi.org/10.1175/JCLI-D-18-0237.1

Wassmann, P., Kosobokova, K. N., Slagstad, D., Drinkwater, K. F., Hopcroft, R. R., Moore, S. E., et al. (2015). The contiguous domains of Arctic Ocean advection: Trails of life and death. *Progress in Oceanography*, *139*, 42–65. https://doi.org/10.1016/j.pocean.2015.06.011

Woodgate, R. A. (2018). Increases in the Pacific inflow to the Arctic from 1990 to 2015, and insights into seasonal trends and driving mechanisms from year-round Bering Strait mooring data. *Progress in Oceanography*, *160*, 124–154. https://doi.org/10.1016/j.pocean.2017.12.007

Zhao, M., Timmermans, M.-L., Cole, S., Krishfield, R., & Toole, J. (2016). Evolution of the eddy field in the Arctic Ocean's Canada Basin, 2005–2015. *Geophysical Research Letters*, *43*, 8106–8114. https://doi.org/10.1002/2016GL069671